www.csiro.au

IMOS Integrated Marine Observing System

Ocean Colour Sub-Facility

Ocean Colour Validation Report

2015-16

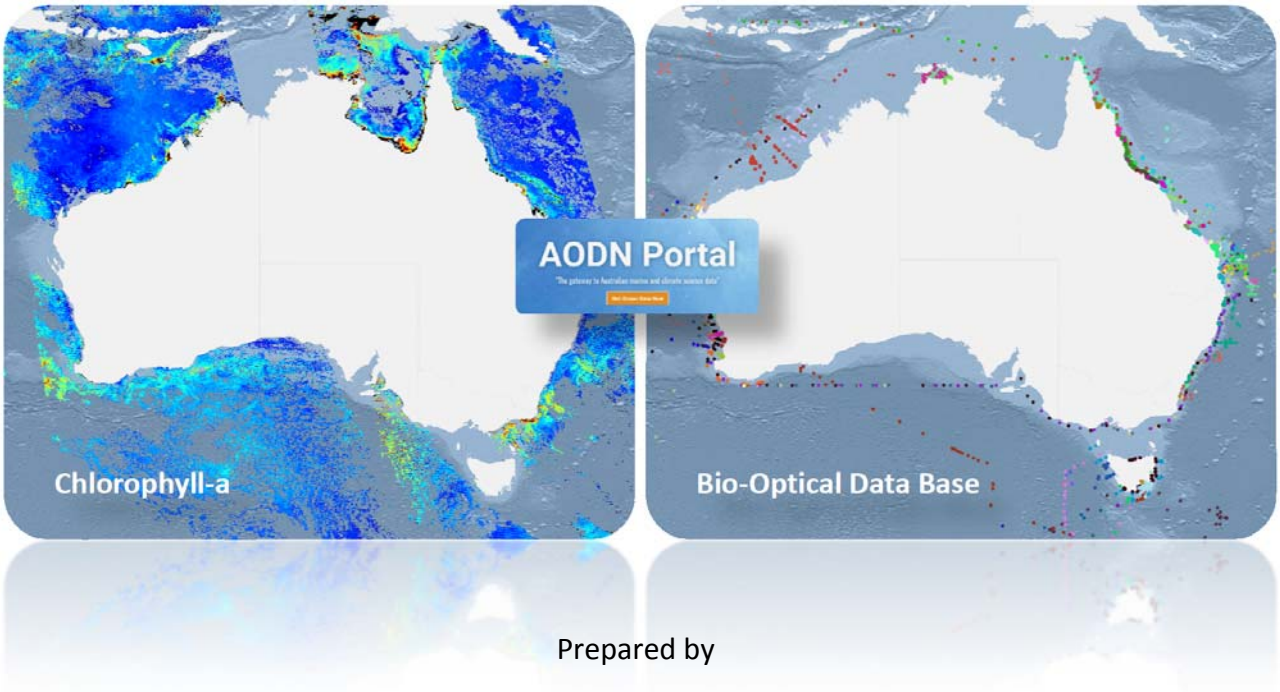

Prepared by

Thomas Schroeder, Jenny Lovell, Edward King, Lesley Clementson, Roger Scott

CSIRO Oceans and Atmosphere

June 2016

NCRIS National Research Infrastructure for Australia
An Australian Government Initiative

UNIVERSITY of TASMANIA

Citation

Schroeder T., Lovell J., King E., Clementson L., and Scott R., (2016), IMOS Ocean Colour Validation Report 2015-16, Report to the Integrated Marine Observing System (IMOS), CSIRO Oceans and Atmosphere, 33 pp.

Copyright and disclaimer

Important disclaimer

Cover Images

Snapshots of the Australian Ocean Data Network (AODN) Portal displaying two subsequent MODIS-Aqua orbits of GSM chlorophyll-a around Australia (left) and the corresponding spatial distribution of IMOS Bio-Optical Data Base measurements.

Contents

Figures

Tables

1 Introduction

Ocean colour observations have been routinely available from NASA satellites for nearly two decades; initially with the launch of the SeaWiFS sensor in 1997 (NASA), then MODIS Aqua in 2002 (NASA) and, more recently, with VIIRS on Suomi-NPP launched in 2012 (NASA/NOAA).

Data from these missions are distributed by the space agency at different processing levels usually ranging from Level 0 (raw unprocessed instrument data) to Level 3 quality that provide derived geophysical products (Level 2) mapped onto uniform space-time grid scales.

While NASA has sought to make products from these missions available at different processing levels and spatial resolutions, their Level 3 data have typically been spatially binned and mapped at approximately 4 or 9 km resolution globally and often are also time-averaged.

These time and space aggregated Level 3 data are convenient for the use in time-series studies or the assimilation into biogeochemical models (BGCM). However, coarser resolution data are often less suitable for coastal applications, developing regional algorithms, or for characterising product accuracy through *in situ* match-ups, where finer spatial resolution data is required.

To address these needs, IMOS has supported the assembly of Australasian archives of raw data from the above mentioned satellite missions and established an Ocean Colour processing system, based on NASA's standard ocean colour processing software SeaDAS (Fu et al., 1998), at the National Computational Infrastructure (NCI).

The IMOS Ocean Colour processing system provides:

- whole-of-mission temporal coverage for the wider Australasian region ([10°N,80°E]-[60°S,180°E])
- ability to reprocess whole-of-mission data, with up to date calibration without need to download from overseas
- full resolution geophysical products (1km for SeaWiFS and MODIS, 750m for VIIRS) unmapped in swath format for match-up analyses
- a large suite of outputs such as reflectance at mean sea level, ancillary and diagnostic products to support new algorithm development
- selected daily mapped continental-scale full-resolution products

Product validation specific for the Australasian region cannot be provided by NASA as most of their products have been developed for global applications and as such NASA's validation efforts focus is on a much broader, global-scale. To enable regional evaluation of satellite ocean colour products IMOS has also supported the collation of a Bio-Optical Data Base (BODB). The BODB collates *in situ* discrete physical, bio-geochemical, and optical data collected by the Australian bio-optical community from 1997 to date in the Australasian region. Product validation is achieved through match-up analysis, comparing a specific satellite product at the locations of the ground observations. However validation data are not available in every region and some marine areas around Australia are sparsely or not at all covered by ground measurements. To enable product validation in these under-sampled regions, the Ocean Colour Sub-Facility has adopted a validation approach that is based on a classification of optical water types (OWT, Moore et. al 2009). This approach assumes that the match-up results obtained for a given water type can be used to estimate the accuracy of a specific product in the absence of ground observations with the help of a corresponding satellite-derived water type map. Water type maps are produced by IMOS as a separate ocean colour product to guide this accuracy interpretation.

This report describes the water type-based validation results of four IMOS generated and distributed chlorophyll-a (chl-a) products in the Australasian marine region.

2 Satellite Ocean Colour Data

2.1 Satellite Data Processing Workflow

IMOS maintains a national collection of MODIS and VIIRS satellite data at the National Computing Infrastructure (NCI). The collection begins with Level 0 (raw) data, processed to Level 1b (geolocated, top of atmosphere radiances), and then to a suite of Level 2 Ocean Colour Radiometry (OCR) products that include atmospherically corrected surface reflectance and many derived in-water products, all at full spatial and temporal resolution. The processing of contemporary data uses the most up to date versions of the SeaDAS MODIS and VIIRS calibration tables and the collection is regularly reprocessed (see below) to ensure the products are as close to the best-available as is practical. Both MODIS-Aqua and MODIS-Terra archives are maintained up to Level 1b. Only data from MODIS-Aqua, the Ocean Colour Radiometry (OCR) enhanced sensor, is carried through the OCR processing chain to Level 2 and Level 3. The MODIS-Terra data is used separately by the Australian Terrestrial Ecosystem Research Network (TERN)[1].

2.1.1 RECENT AND PAST ARCHIVE SEPARATION

The L1b archive is very large, of the order of 90TB and approximately 350,000 granules for both MODIS satellites (roughly half that for Aqua alone), so a full reprocessing is a very significant and computationally intensive undertaking. Although calibration updates are made relatively frequently by the NASA group, their impact is nearly always concentrated in the most recent months or years, with the changes blending smoothly back into previous calibration releases a few years before the present. Accordingly it is less critical to reprocess the earlier part of the collection frequently. To facilitate this, and to make the distinction explicit, the archive is split into a 'Recent' component and a 'Past' component. The 'Recent' component, currently January 2013-present, is reprocessed in full more frequently, whereas the much larger 'Past' component only about once every 12-18 months, usually when there is a significant SeaDAS software upgrade that accounts for advances in algorithms.

Consequently, at any stage, the full time series has to be accessed via two complementary paths. As each reprocessing of the 'Recent' segment occurs, the versions associated with each of these paths differ progressively. For consistency and to aid tracking processing versions, this segmentation is carried through the whole processing chain up to and including the Level 2 product collections. Figure 1 illustrates this and each stage is described in detail in the sections below.

2.1.2 LEVEL 0 STAGE

This collection is created from Level 0 data delivered in near real time from Australian direct broadcast reception stations, augmented by data downloads from NASA. The MODIS Level 0 data files are in a format known as Production Data Sets, or PDS. NASA distributes PDS files starting at UTC 5 minute intervals (on the hour, 5 minutes past, 10 minutes past, and so on), each of which contains an image granule of 5-minutes duration. In contrast the Australian reception stations record and deliver a continuous swath of a length closely matching the duration with which the spacecraft was in line-of-sight of the station.

Upon receipt of an overpass from a reception station, the ingest system at the NCI splits the pass into 5-minute chunks with boundaries on 5-minute intervals matching the NASA granules. The system maintains a short rolling archive, a near real time (NRT) collection, of a few weeks duration into which new granules, or

[1] http://portal.tern.org.au/

fragments of granules (whether from reception stations or NASA) are merged as they arrive. The merging software is based on C code developed by Dr Stefan Maier (formerly of Landgate in Perth and Charles Darwin University). This rolling archive is the most complete and up to date collection of Australian PDS granules. Through a series of continuously updated symbolic links in the NCI filesystem, this NRT archive is merged into the 'Recent' collection of PDS data. The 'Recent' collection, of 2-3 years duration, is kept online to facilitate reprocessing. The 'Past' collection of PDS data is stored offline at the NCI since it is usually only required every 1-2 years when a whole of archive reprocessing occurs.

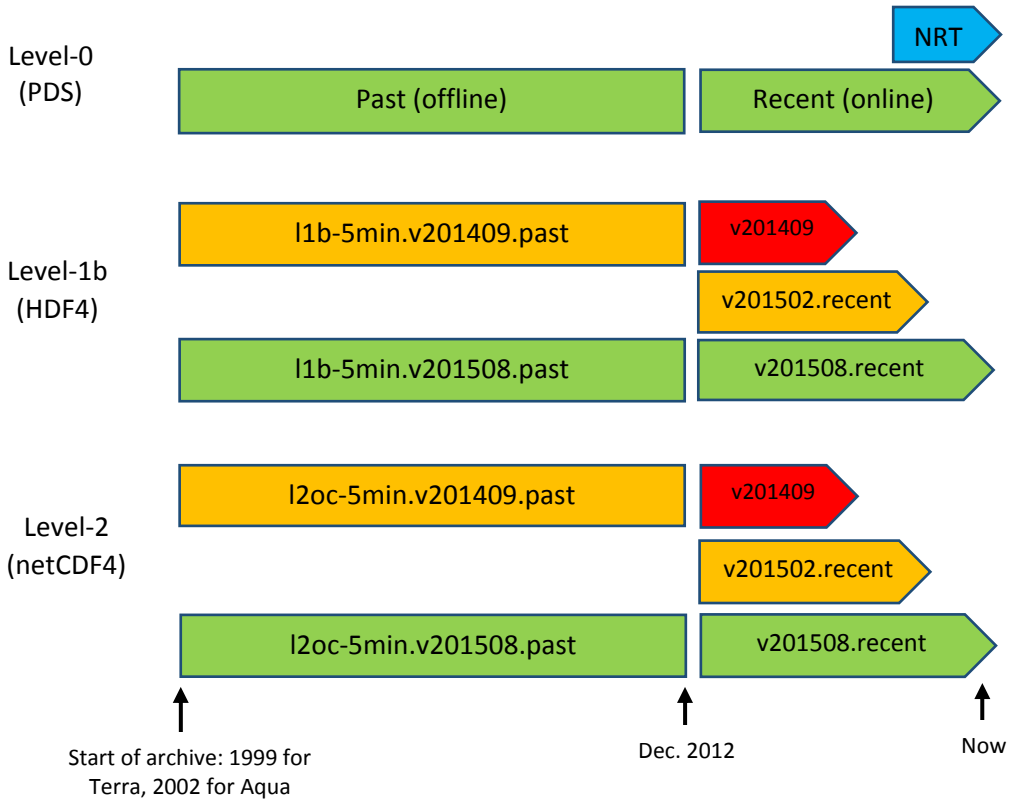

Figure 1 The segmentation of the archive into 'Past' and 'Recent' carries right through the processing chain to Level 2. The 'Past' collection is updated less frequently than the 'Recent' collection. Only the green components (the latest processing at each level) are active at any time. The red and orange components are obsolete and are usually removed from the system once they have been superseded. The version number (vYYYYMM) encodes the four digit year and two digit month in which the collection processing commenced.

2.1.3 LEVEL 1B STAGE

The Level 1b data sets, which include geolocation information and calibrated top-of-atmosphere radiances for each channel, are computed from the Level 0 data using the MODISL1DB v1.8 package included in SeaDAS and are in HDF4 format. Level 1b is the processing step where the calibration is used, and it is therefore the point from which reprocessing has to begin when the calibration is significantly updated (Figure 1).

It is possible to compute the Level 1b immediately from the PDS files using predicted spacecraft ephemeris but, as operated, the system is configured to wait until the definitive ephemeris is available. In practice this occurs usually 12-18 hours after the satellite overpass. Once the definitive ephemeris is available the PDS granules are processed to Level 1b. This step can occur more than once if the PDS granule is subsequently updated by a late-arriving station or NASA data set.

Complete Level 1b archives are maintained for both Aqua and Terra, and for day and night time granules. The night time files are only 20% the size of the day time files since there is no data in the reflectance channels; they are created to enable production of sea surface temperature products that depend only on the thermal channels.

True-colour imagery is also produced from the Level 1b day time data granules. This is done following the method outlined by Gumley[2] (2010), yielding a 250m resolution image using two sharpened 500m bands and a generic Rayleigh atmospheric correction. There is a complete set of true colour imagery for both Aqua and Terra from the Past collection available at the NCI remote sensing web server[3]. The True colour imagery is not yet complete for the 'Recent' collection.

2.1.4 LEVEL 2 STAGE

The Level 2 processing is undertaken with the SeaDAS *l2gen* module and produces files in netCDF4 format. *L2gen* applies the standard atmospheric corrections to obtain water-leaving radiances. These are used in turn to produce remote sensing reflectance to which all manner of in-water retrieval algorithms can be applied. As mentioned above, the Level 2 processing is applied only to the Aqua day time data. The present 'Recent' archive uses *l2gen* from SeaDAS v7.3.1.

The Level 2 processing requires several ancillary data files that provide time varying information about the atmosphere (e.g. ozone and water vapour) and ocean surface (e.g. temperature). The processing does not take place until these become available, typically on a similar timescale to the definitive ephemeris. However it is not uncommon for these files to be delayed further, or to be updated after a few days. In the latter instance, this is detected and the Level 2 processing is repeated using the updated files to ensure the best quality data is available as soon as possible.

The Level 2 Aqua data files contain the water leaving radiances, remote sensing reflectances, and a myriad of derived products, all at 1km resolution and in satellite projection (*i.e.* unmapped). The main chl-a products available are *chl_oc3, chl_gsm, chl_carder, and chl_oci* (see Section 2.2) together with (an evolving list of) many other products. Because the Level 2 data have not been remapped, the match-up extractions for comparison against the *in situ* measurements are extracted from this tier of the processing.

2.1.5 LEVEL 3 PRODUCTS

The final processing step is to re-grid the Level 2 data onto a rectangular longitude-latitude map projection, and to merge all the granules from each day to form a national mosaic. The map grid is set to a step size of 0.01 degree and the map coverage is the greater Australasian region (e.g. Figure 2). The data are in netCDF4 format and are exported for further distribution by IMOS. The distinction between 'Recent' and 'Past' collections is not made for the Level 3 products, since the difference should be undetectable and most users of these data are interested in a continuous time series.

2.1.6 VIIRS DATA PROCESSING SYSTEM

A similar L0-L1b-L2 processing workflow has been implemented for VIIRS, which uses the same SeaDAS software v7.3.1. The archive is currently not segmented into a 'Past' and 'Recent' processing series due to the much shorter time series of this mission.

[2] https://earthdata.nasa.gov/files/MODIS_True_Color.pdf
[3] http://remote-sensing.nci.org.au/u39/public/data/modis/l1b-5min.true-colour

2.2 Brief description of chlorophyll-a algorithms

The chl-a algorithms used in this validation exercise were two empirical algorithms, *OC3* (O'Reilly et al., 2000) and *OCI* (Hu et al, 2012, Wang and Son, 2016) together with two semi-analytic algorithms, *GSM* (Maritorena et al., 2002) and *Carder* (Carder et al., 1999, 2003). *OC3* is a 3-band empirical polynomial model based on regressions with the NOMAD version 2 dataset[4]. *OCI* is based on a colour index, defined as the difference between remote-sensing reflectance (Rrs) in the green and a reference formed linearly between Rrs in the blue and red. It was specifically designed to improve the retrieval of low concentrations of chl-a (<0.25mg m^{-3}) relative to *OC3* retrievals. The SeaDAS implementation of this algorithm merges it with the *OC3* algorithm over the chl-a range 0.25-0.3 mg m^{-3}, and the derived concentrations above 0.3 mg m^{-3} are identical for *OC3* and *OCI*. The *GSM* model simultaneously retrieves the concentration of chl-a, as well as the combined absorption coefficient due to dissolved and detrital materials and the particulate backscatter coefficient from the normalized water leaving radiance spectrum. The *Carder* algorithm is an inversion of the remote sensing reflectance spectrum to retrieve chl-a concentration along with absorption due to phytoplankton and gelbstoff, however several model parameters are either fixed or specified for a particular region or season.

Figure 2 displays the median *OC3* values for February 2014, illustrating the spatial extent covered by the IMOS Ocean Colour processing system and the approximate range of chl-a concentrations present in the region.

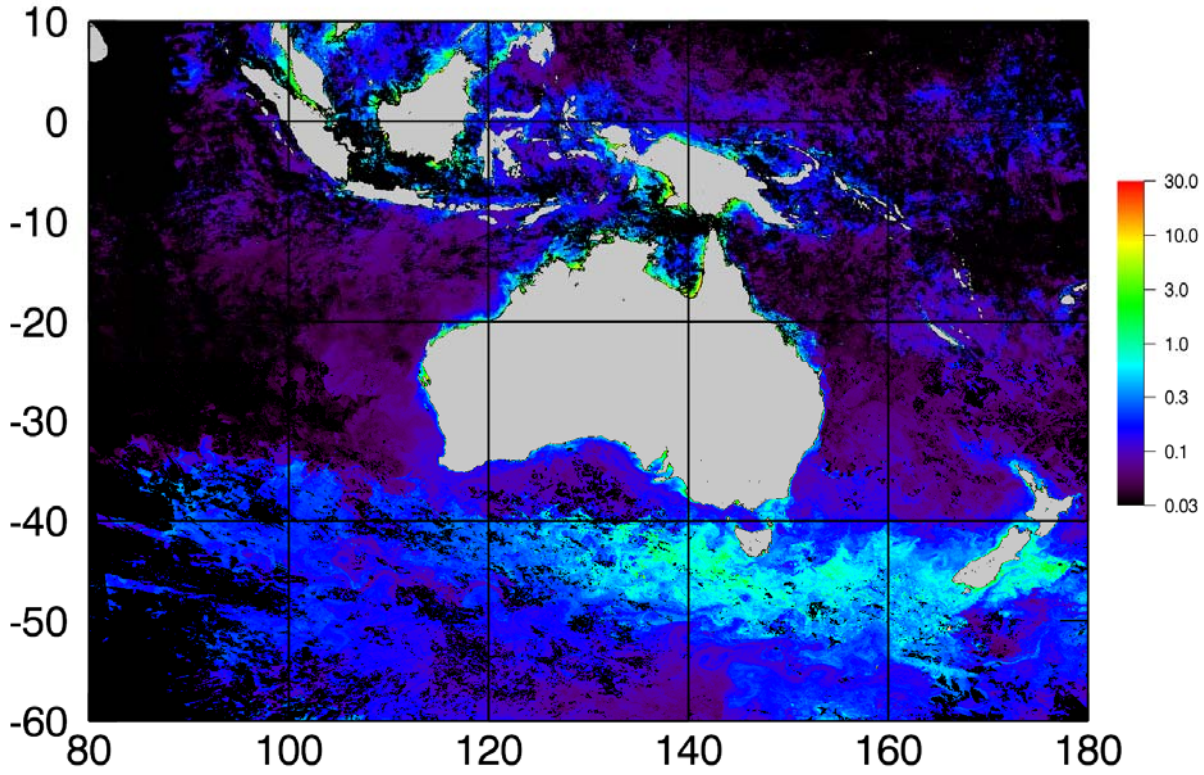

Figure 2 MODIS-Aqua monthly median *OC3* chl-a concentration (units in mg m^{-3}) for the month of February 2014.

[4] http://seabass.gsfc.nasa.gov/wiki/article.cgi?article=NOMAD

2.3 Optical Water Types product and classification

Historically, ocean waters have been broadly classified into *Case 1* and *Case 2* for the purposes of algorithm development and uncertainty analysis (IOCCG, 2000). Moore et al. (2009) took the approach of classifying a global set of *in situ* radiometric measurements into eight distinct water types defined by their optical properties. Figure 3 shows the mean spectra of each optical water type (OWT) cluster, ranging from low chl-a blue-waters (types 1 and 2) to turbid, sediment and CDOM-dominated waters (types 5-8).

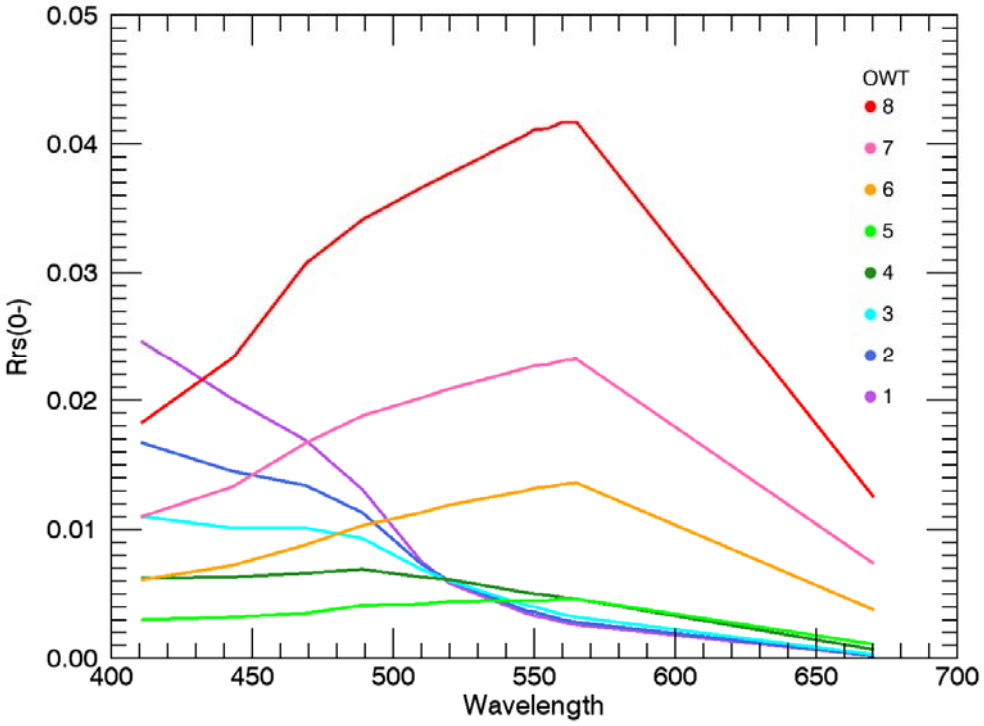

Figure 3 Optical Water Type spectra from Moore et al (2009).

The motivation for Moore's classification was to develop a framework for characterization of uncertainty distributions for ocean colour products. In remotely sensed data, the optical water type is a statistical property of the remote sensing reflectance spectrum. Thus, if uncertainty in a product is catalogued according to OWT, the uncertainty distribution map can be created dynamically at the native resolution of the observed remote sensing reflectance.

In this report, we have a spatially-limited set of *in situ* measurements for validation of the satellite-derived ocean colour products. To enable extension of the uncertainty assessment to regions that are currently not covered by *in situ* sampling, we provide summary statistics on the accuracy of the chl-a algorithms classified by OWT.

An example map of dominant OWT classified with MODIS remote sensing reflectance is shown in Figure 4. We see the large ocean basins dominated by types 1 and 2; shelf waters of types 3 and 4; and coastal regions ranging from types 5-8. Such maps can provide accuracy information in regions with insufficient validation data by using an OWT climatology or classification of the daily reflectance data.

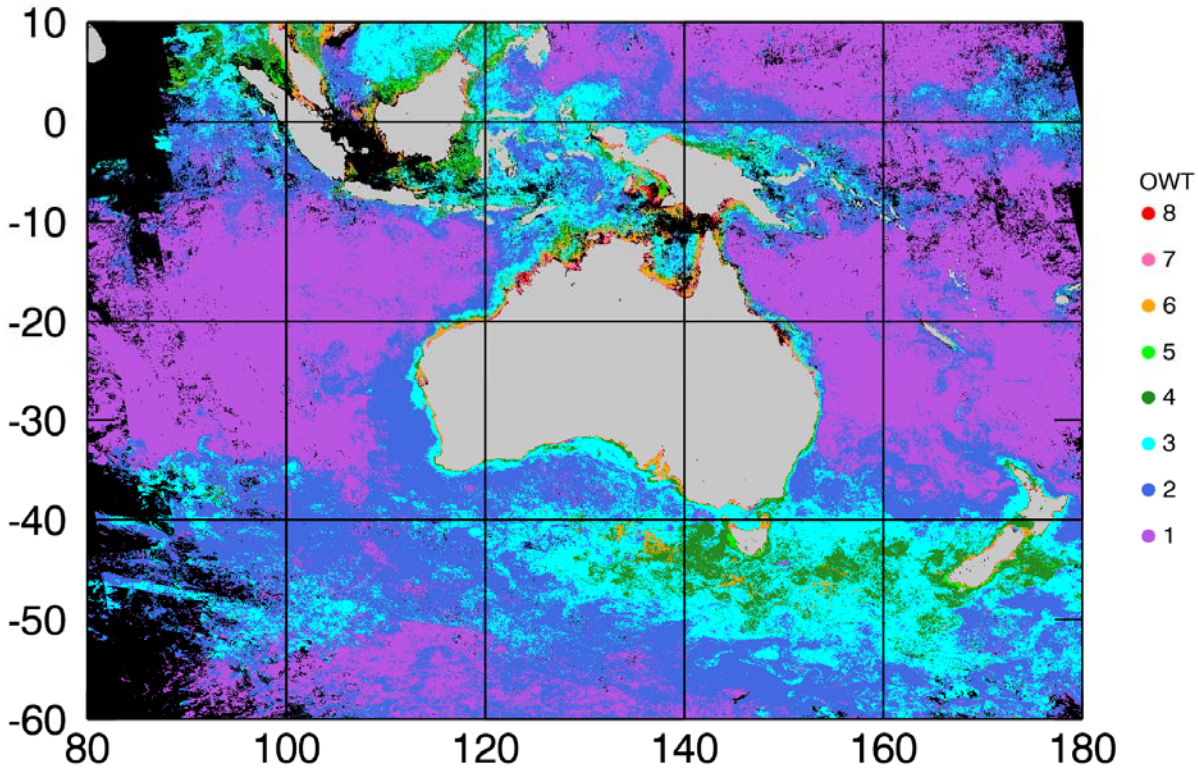

Figure 4 Most common Optical Water Type for each satellite grid point of Figure 2 (February 2014).

The Moore (2009) classification of optical water types has been implemented for MODIS processing in SeaDAS. However, the SeaDAS OWT implementation is based on only three MODIS bands and is not available for VIIRS.

The sample set used in this study is dominated by coastal waters of varying complexity, thus to take account of the full wavelength range of the satellite data the 8-class OWT classification was implemented separately. A classification for both MODIS and VIIRS was implemented by the IMOS Ocean Colour Sub-Facility using six bands for MODIS and five bands for VIIRS. Statistical results (see Appendix B are presented for each optical water type for MODIS. However, in this initial report there are insufficient numbers of match-ups for VIIRS to allow separation into water types.

3 Validation data and match-up analysis

3.1 The IMOS Bio-optical Data Base

IMOS supports the Bio-optical Data Base, which is publicly available through The Australian Ocean Data Network (AODN) portal (https://portal.aodn.org.au/). This data base is a repository of Inherent Optical Properties (IOPs) collected from primarily Australian waters between the mid 1990's to the present day. The IOPs include pigment composition and concentration, TSS concentration, absorption coefficients for the dissolved (a_{CDOM}) and particulate (a_p, a_{ph} and a_d) fractions of the water column and backscatter coefficients. This data set can be used for satellite retrieved product validation, such as chl-a, Coloured Dissolved Organic Matter (CDOM) and suspended sediment concentration or for the development of regional ocean colour algorithms.

3.2 Chlorophyll-a data

Chl-a concentration is often used as an indicator of phytoplankton biomass and is one of the main products of satellite ocean colour data. Chl-a concentration can be measured in several ways, but the most accurate method is High Performance Liquid Chromatography (HPLC), which separates chl-a from its isomers and allomers and from degradation derivatives, such as chlorophyllide-a, phaeophorbide-a and phaeophytin-a. Other methods include spectrophotometric analysis, where chl-a is determined from a series of spectrophotometric equations developed by Jeffrey and Humphrey (1975) and spectrofluorometric analysis where the spectrofluorometer has been calibrated with a chl-a standard solution. In both methods the chl-a concentration will include contributions from the isomers, allomers and degradation derivatives and are therefore less accurate. Further discussion of these techniques can be found in Neveux et al (2011).

3.3 Match-up extraction

The objective of match-up extraction is to identify the satellite observations to be compared with *in situ* measurements[5] – to 'match-up the satellite with the surface data' – so that an assessment can be made of the degree to which the remotely sensed observation is able to represent the at-surface conditions.

Ideally we would like to identify a single satellite pixel at exactly the location of the surface measurement and at the precise time that the measurement was made. There are however several confounding issues that make this task challenging.

Firstly the *in situ* measurement may not have been collected at the exact time of the satellite overpass. Secondly there may be clouds, or some other optical phenomenon (such as glint from the sun) present which obscure the surface location observed by the satellite. Thirdly a satellite pixel, by its very nature, is not an observation at a point but a weighted average over some larger area of metres to kilometres. In comparison, an *in situ* measurement is usually confined to a relatively small area, typically a few metres or even less.

In practice these difficulties are overcome by making a (subjective) assumption about the spatial homogeneity, and the rate of change in time, of the surface property being measured. This enables satellite observations at different times or nearby the *in situ* measurement to be utilised, with the caveat that there may be some loss of fidelity in the comparison. To an extent, this loss can be assessed by examining a group

[5] Although the terms are completely interchangeable, for clarity we shall adopt the convention of referring to the satellite data as 'observations' and the *in situ* data as 'measurements' throughout this section.

of nearby satellite pixels for mutual consistency; if they are significantly different from each other then the assumption of homogeneity is unlikely to be valid.

Lastly the degree of processing of the satellite data can have an impact on the validity of the comparison. Satellite observations, which are collected on a regular grid from the perspective of the sensor (itself a moving platform), are commonly transformed (or re-gridded) to a conventional map grid on the surface of the Earth for ease of use. We refer to these two grids as the *swath grid* and the *map grid* respectively. The issue arises that the re-gridding process, depending on the exact sampling technique, moves each observation slightly from its original location to a nearby location on a discrete map grid, and possibly combines it with other nearby observations in an attempt to account for the movement. Consequently re-gridded data will almost always compromise the fidelity with which the decision about which pixel(s) best represent the surface measurement can be made. For this reason it is always preferable to seek the satellite match-up observations in the swath (un-remapped) images. For some sensors (such as MODIS and VIIRS) this approach complicates the analysis somewhat because the relationship between the swath and map grids is not straightforward (see Section 3.4).

Figure 5 illustrates the match-up process. Potential satellite imagery that is likely to contain *in situ* measurement of relevance is identified from the satellite archive. This search is guided by the time and location of the *in situ* measurement together with a time range and a specification of the linear size of the box of pixels to be extracted surrounding the *in situ* location. The initial result is a mini-granule of satellite data, (with multiple channels of spectra and/or derived products and data quality information) which includes the group of satellite pixels surrounding the *in situ* measurement location. This mini-granule is extracted because it is much smaller than the full image and is more easily managed during the subsequent analysis.

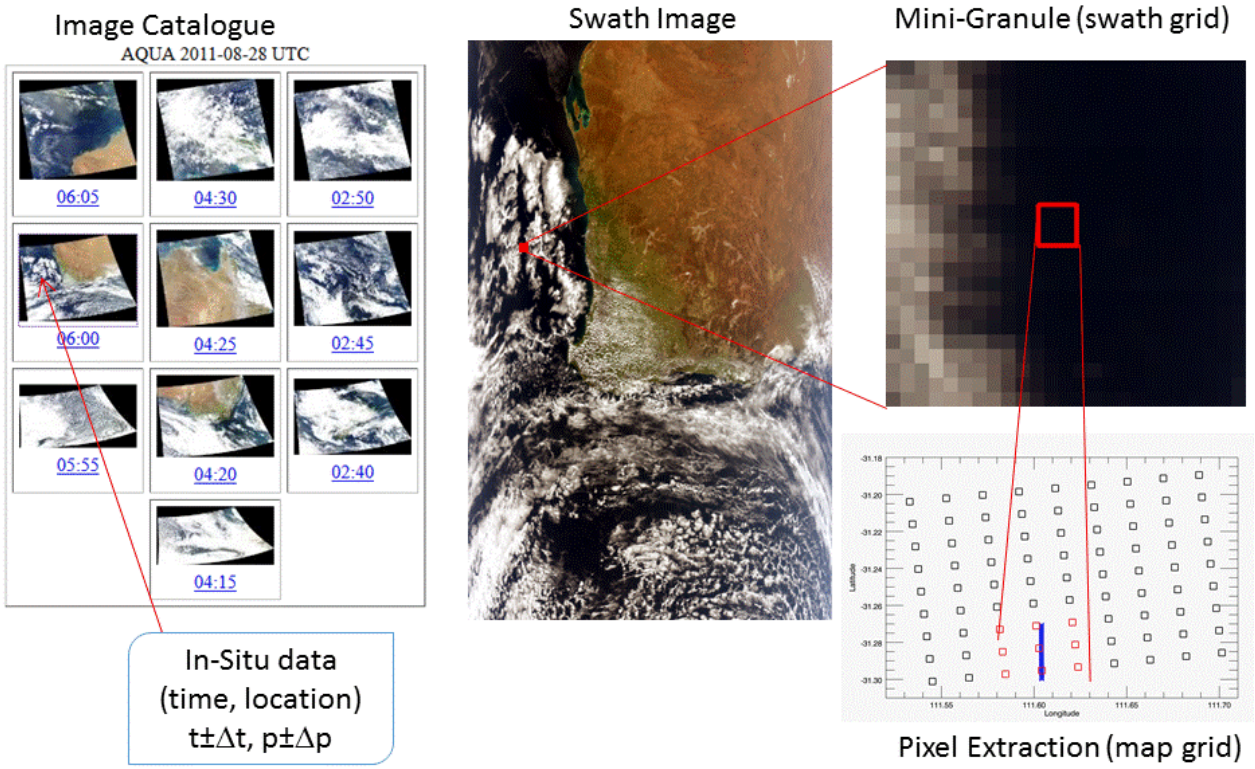

Figure 5 Illustration of the match-up process. Firstly the satellite scene covering the *in situ* measurement location and closest in time is identified. The swath file is then searched for the group of pixels surrounding the *in situ* location (red dot) and those data are extracted to a mini-granule for further analysis. Selection of the actual pixels to use from the mini-granule is based on consideration of distance and quality thresholds on a per-pixel basis. In this example the *in situ* measurement lies on a ship track (blue line) and the chosen pixels are indicated in red. Although all the computation takes place in a swath grid, this last step is illustrated on a map projection for clarity.

The main processing steps of the match-up extraction are as follows:

1. A table with all available *in situ* chl-a measurements is compiled from the IMOS Bio-optical Data Base, applying a selection criterion of observation depth less than 10 m. The extracted data set consists of the measurement location, universal time, and the value of the measured chl-a concentration, observation depth and other identifying information. This table of *in situ* measurements is used to identify candidate imagery from the scene catalogue.

2. For each *in situ* measurement, the swath grid in each candidate scene (there may be more than one scene per *in situ* point), is searched for the pixel closest to the *in situ* measurement. This search begins at the scene centre and quickly localises using a gradient descent. Once the gradient step size decreases below a threshold (indicating near-convergence), a brute force search for the actual closest pixel is conducted by examining the distance to every pixel in an enclosing rectangular box. This step is necessary because the gradient descent may behave unpredictably where the bow-tie effect becomes significant.

3. A mini-granule of sufficient size to include all potentially relevant pixels (21x21) is extracted from the swath grid, centred on the pixel closest to the *in situ* measurement.

4. For convenience, an index is written to the mini-granule that provides access to each pixel in the mini-granule in order of increasing distance from the *in situ* measurement location.

5. The mini-granule, *in situ* measurement and ancillary information are stored in a netCDF file.

6. Valid match-ups are retained if the 3x3 pixel subset centred on the closest pixel contained at least 5 valid pixels after applying quality control flags. A pixel may become invalid due to algorithm failure or due to the present of atmospheric or oceanic conditions that cannot be corrected for (e.g. sun glint). Data quality control flags are computed by *l2gen* as a separate product and are provided in form of a 32-bit mask. The following bit masks listed in Table 1 are used to quality control the match-up extractions.

7. Match-up are initially extracted at a maximum time difference of ±24 hours between the in-situ and the satellite observations, which allow further sorting into smaller time differences as required.

Table 1 Level 2 quality control flags (bit masks) applied during the match-up extraction process.

Bit	Description
1	Atmospheric correction failure
2	Pixel is over land
4	Sun glint: reflectance exceeds threshold
5	Observed radiance very high or saturated
6	Sensor view zenith exceeds threshold
10	Probable cloud or ice contamination
12	Solar zenith exceeds threshold
16	Chlorophyll algorithm failure
22	Chlorophyll out of bounds
26	Navigation quality is suspect

3.4 The bow-tie effect

The MODIS and VIIRS sensors share a design feature that complicates working in the swath grid. They collect observations with a scan direction perpendicular to the ground track using not a single detector but a group; ten in the case of MODIS, and sixteen for VIIRS. At nadir, at the sub-satellite point, the pixels cover adjacent ground locations. As the scan progresses away from nadir however, geometrical effects result in the pixels growing in size at the surface, creating an overlap between successive scans of the *groups* of pixels near the scan edges leading to a shape across the full width of the image reminiscent of a bow-tie (Figure 6).

To appreciate what impact this has on the analysis of the imagery spatially, it is useful to examine the effect on the remapped imagery (Figure 7). Adjacent pixels in the swath image (from which we prefer to select observations for match-up analysis) are not necessarily adjacent on the ground. Not only can there be interleaved pixels from an adjoining scan group, but the first detector row in one group can occur prior on the ground to the last detector row of the previous group.

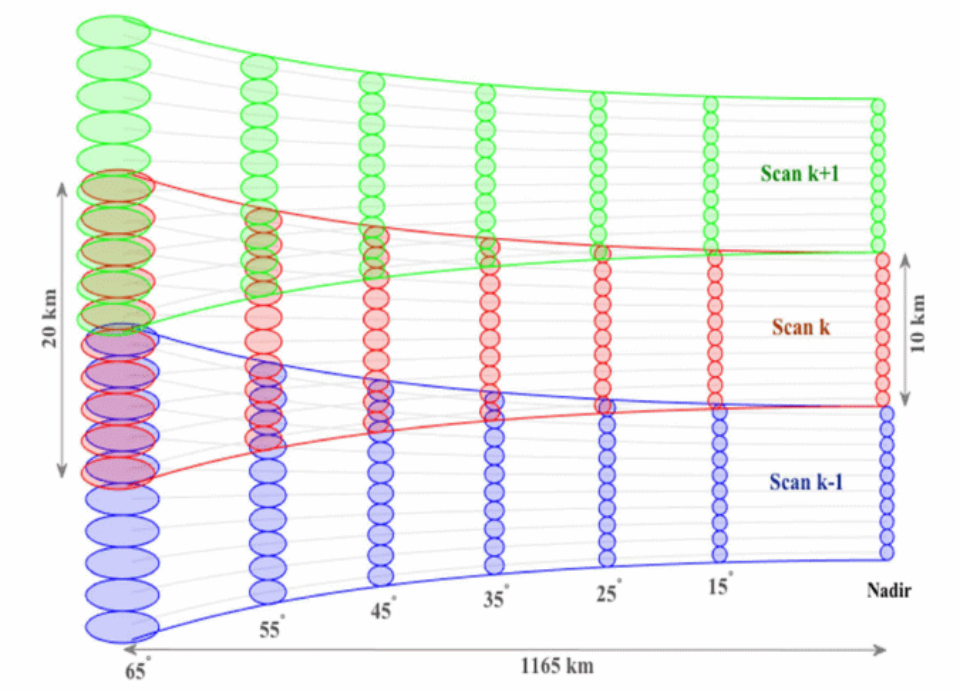

Figure 6 The MODIS 'bow-tie' effect illustrated on one side of the swath for three successive scans of the group of 10 detectors. Although somewhat exaggerated, the bow-tie shape is clearly visible. Figure reproduced from Figure 12 of Gladkova et al. (2016).

The examples shown are for the MODIS 1km detectors. For the 250m channels, the groups comprise 40 detectors. This is no more complicated, but failure to take it into account will be relatively more severe due to the decreased pixel size. In practice match-ups are not normally accepted from the extreme swath edges (because the greater atmospheric path length increases the observational uncertainty due to atmospheric correction limitations) however it is clear, from Figure 7c, that the bow-tie effect is important even halfway to the swath edge. Figure 7c and Figure 7d also illustrate why it can be unsatisfactory to select match-up pixels from the map grid, since there are obviously map grid cells which would contain more than one observation, and so either observations would be discarded, or they would need to be combined in some way.

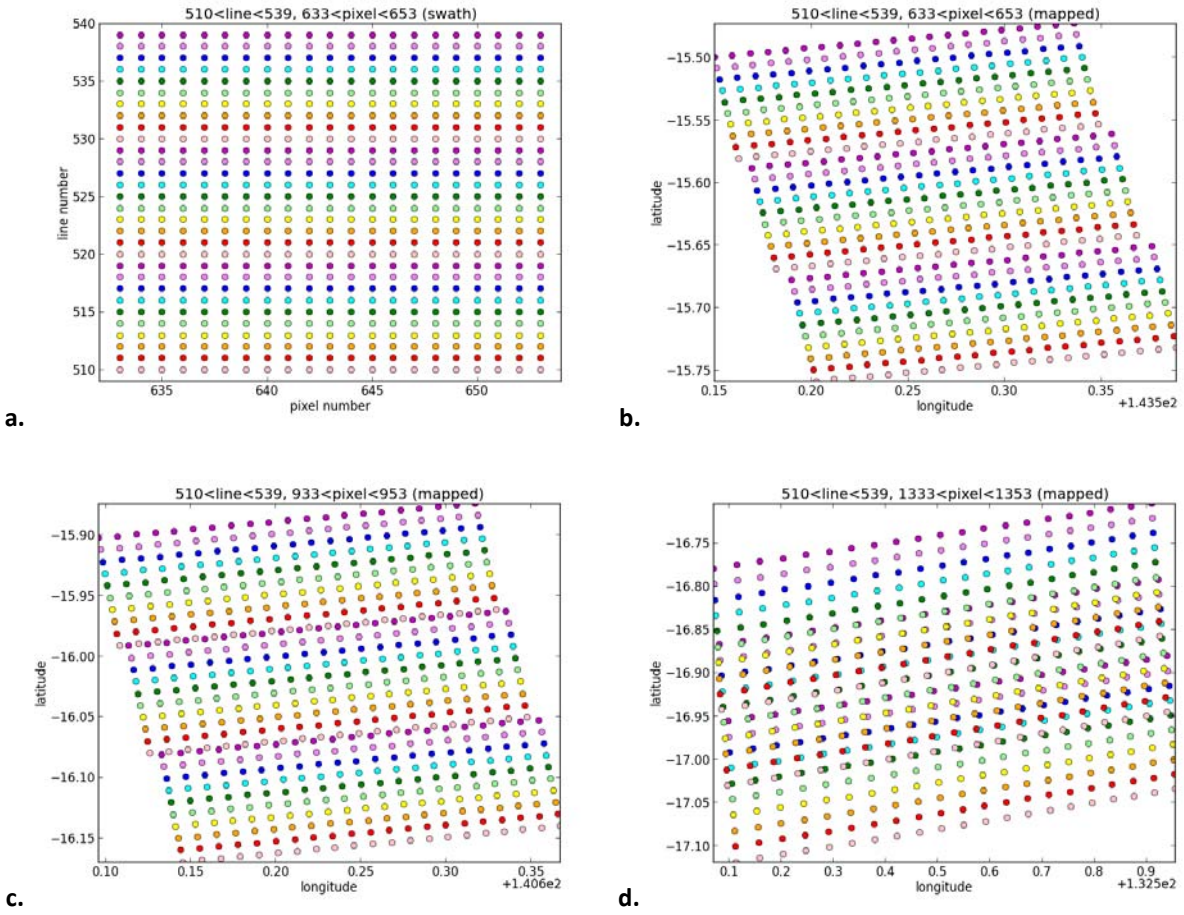

Figure 7 Detail of the bow-tie effect. (a) shows three successive groups of 10 detectors (each separately colour coded) as they are stored in a swath file. Each observation has a corresponding longitude and latitude on the Earth surface but the spatial relationship is not apparent in the swath grid. (b) shows the same pixels on a map grid close to the satellite nadir and illustrates the spatial relationship. (c) is the same as (b) except for a group of pixels midway to the swath edge. The overlap between groups is beginning to emerge. (d) illustrates the effect at the edge of the swath, where it is most severe and all pixels in a scan overlap with those from either the next or previous scan.

4 Results and discussion

This report focused on validation of chl-a retrievals only, using the *OCI*, *OC3*, *GSM*, and *Carder* algorithms applied to MODIS-Aqua and the *OC3* and *GSM* algorithms applied to VIIRS.

In situ chl-a measurements were extracted from the IMOS Bio-optical Data Base for the region bounded by 100°W-180°W longitude and 10°N-60°S latitude within the time period covered by MODIS and VIIRS data. The data comprise 1,182 measurements for MODIS-Aqua (2002-present) and 180 for the VIIRS sensor (2012-present). The spatial distribution of these measurements is illustrated in Figure 8a. These data were matched with satellite overpasses within a temporal window of ±24 hours. After application of quality flags, the resulting number of matched datasets was 716 for MODIS-Aqua and 32 for VIIRS as illustrated in Figure 8b and c, respectively. Larger observational gaps exist for MODIS in the Great Australian Bight and the Gulf of Carpentaria. The match-up data set for VIIRS is small due to the much shorter operation of this sensor and limited to parts of the Great Barrier Reef and the Van Diemen Gulf of the Northern Territory.

Another reason for this data reduction is that the *in situ* data used in this validation study were acquired in a variety of projects with differing objectives and thus the sampling strategies and times are not optimized to coincide with the satellite data acquisition. The OWT of the matched MODIS data are dominated by two types: 40% are type 7 (turbid, coastal) and 30% are type 3 (off-shore, shelf waters). The distribution of matched MODIS observations according to OWT is shown in Figure 9.

Errors and uncertainties that are random in nature are often expressed as a percentage and can be evaluated through the root mean square error (RMSE) or mean absolute percentage error (MAPE). However, there may also be systematic errors that cause bias in the derived algorithm values. In the case of chl-a concentration, the natural distribution of values is log-normal. RMSE and correlation are computed on log-transformed data, while non-transformed values are used for the computation of bias and MAPE (Appendix B We present match-up statistics for each algorithm classified according to the elapsed time between *in situ* and satellite observations (Table 10-Table 13). as well as by optical water type for a match-up window of ±24 hours (Table 2-5) and ±2 hours (Table 6-9) for MODIS. The VIIRS match-up data are extremely sparse and statistics are therefore presented only for a ±24 hour match-up window with all water types combined (Table 14).

Overall, each of the four MODIS chl-a algorithms shows highly significant ($p<0.01$) correlation with the *in situ* data (Figure 10 and Table 10-Table 13). RMSE is slightly lower for the semi-analytic algorithms and MAPE is lowest for *Carder*. However, the error bars in Figure 10 appear larger for the *Carder* and *GSM* algorithms, indicating more significant spatial variability with these algorithms. All algorithms produce chl-a distributions with a positive bias compared with *in situ* data, but the bias in the *Carder* algorithm is much smaller than the other three (Figure 11).

Statistical comparisons differ across the eight OWT classes. All four algorithms show positive bias for OWT6-8 with the largest bias in *OC3* and *OCI* and the smallest in Carder (Table 2-5). In contrast, all algorithms show negative bias for OWT1 and all except *GSM* show negative bias for OWT4. The *GSM* bias is the smallest in both OWT 1 and 4. There is very little bias in *OC3* and *OCI* for OWT 2 and 3 while *GSM* has a larger, positive bias and *Carder* a larger, negative bias.

Highly significant ($p<0.01$) correlations were found for all OWT except for OWT1 for *OCI*, *GSM* and *Carder* and OWT8 for *GSM* and *Carder* (Table 2-5). In the off-shore water types (2 and 3) *OC3* and *OCI* had stronger correlations than *GSM* and *Carder*, while for the more complex waters (6 and 7) *GSM* showed the strongest correlation.

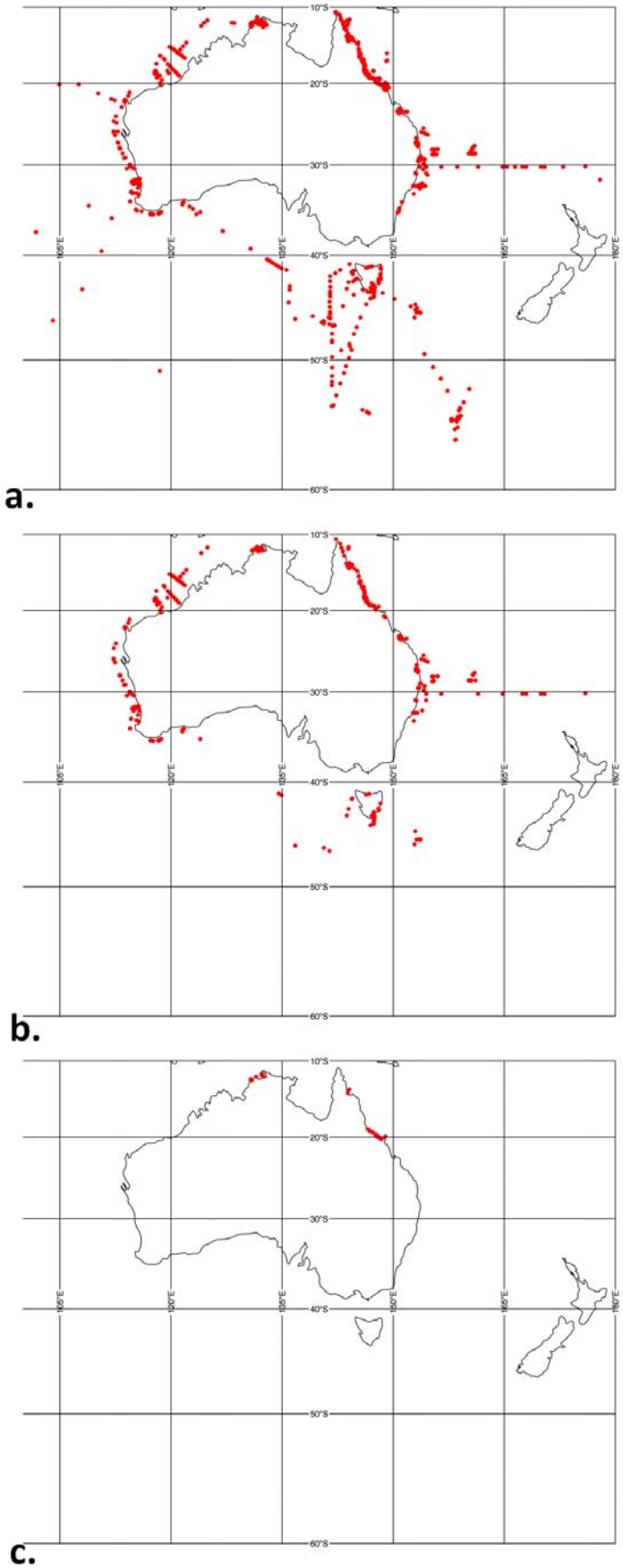

Figure 8 (a) Location of all *in situ* chl-a measurements of the IMOS Bio-optical Data Base starting 1999. (b) Location of *in situ* chl-a measurements matched with MODIS-Aqua observations. (c) Location of *in situ* chl-a measurements matched with VIIRS observations. Maximum time difference ΔT between *in situ* and satellite data for this plot is ±24 h.

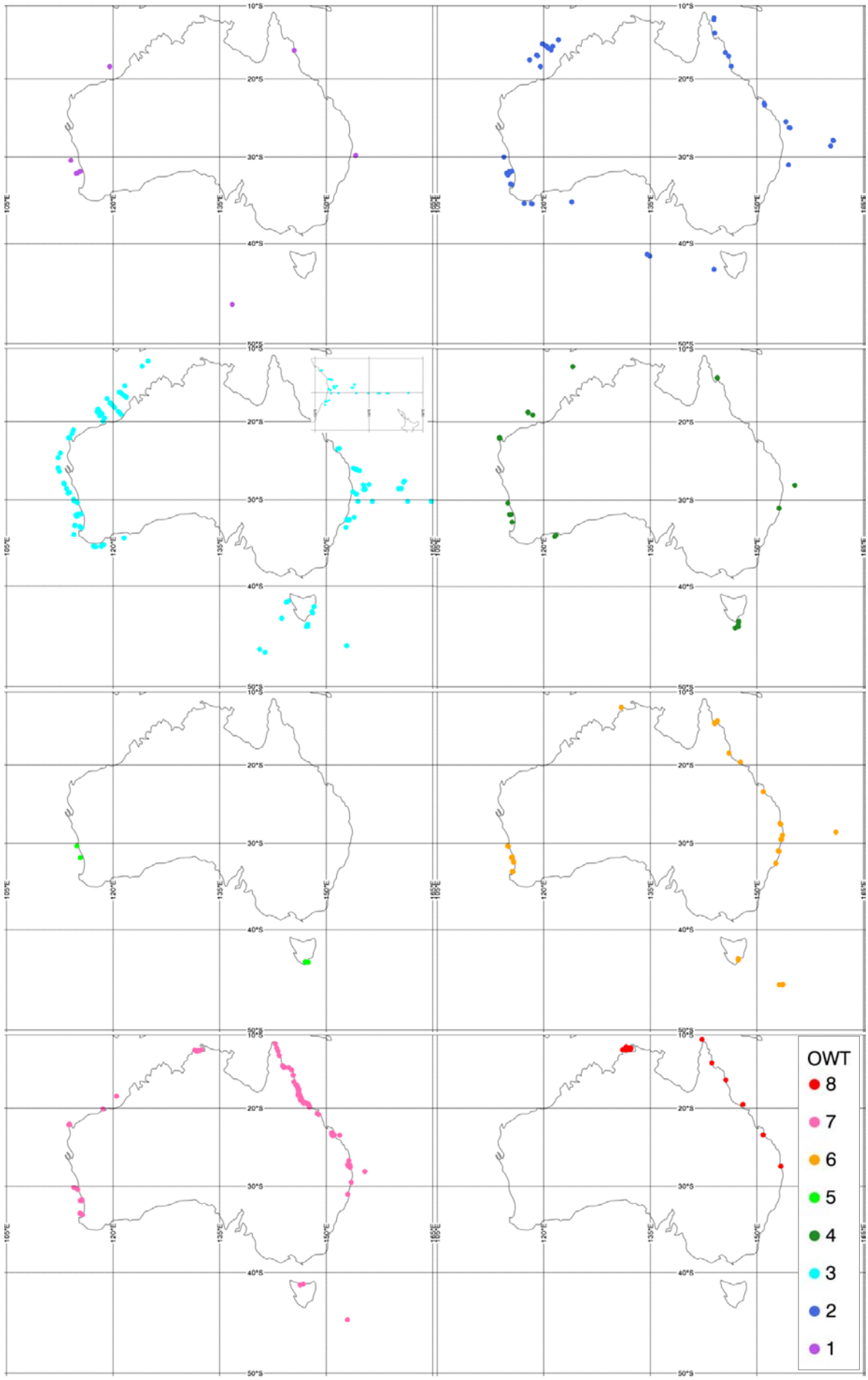

Figure 9 Spatial distribution of MODIS-Aqua chl-a match-up data (Fig 8b) classified by OWT (ΔT=±24 h).

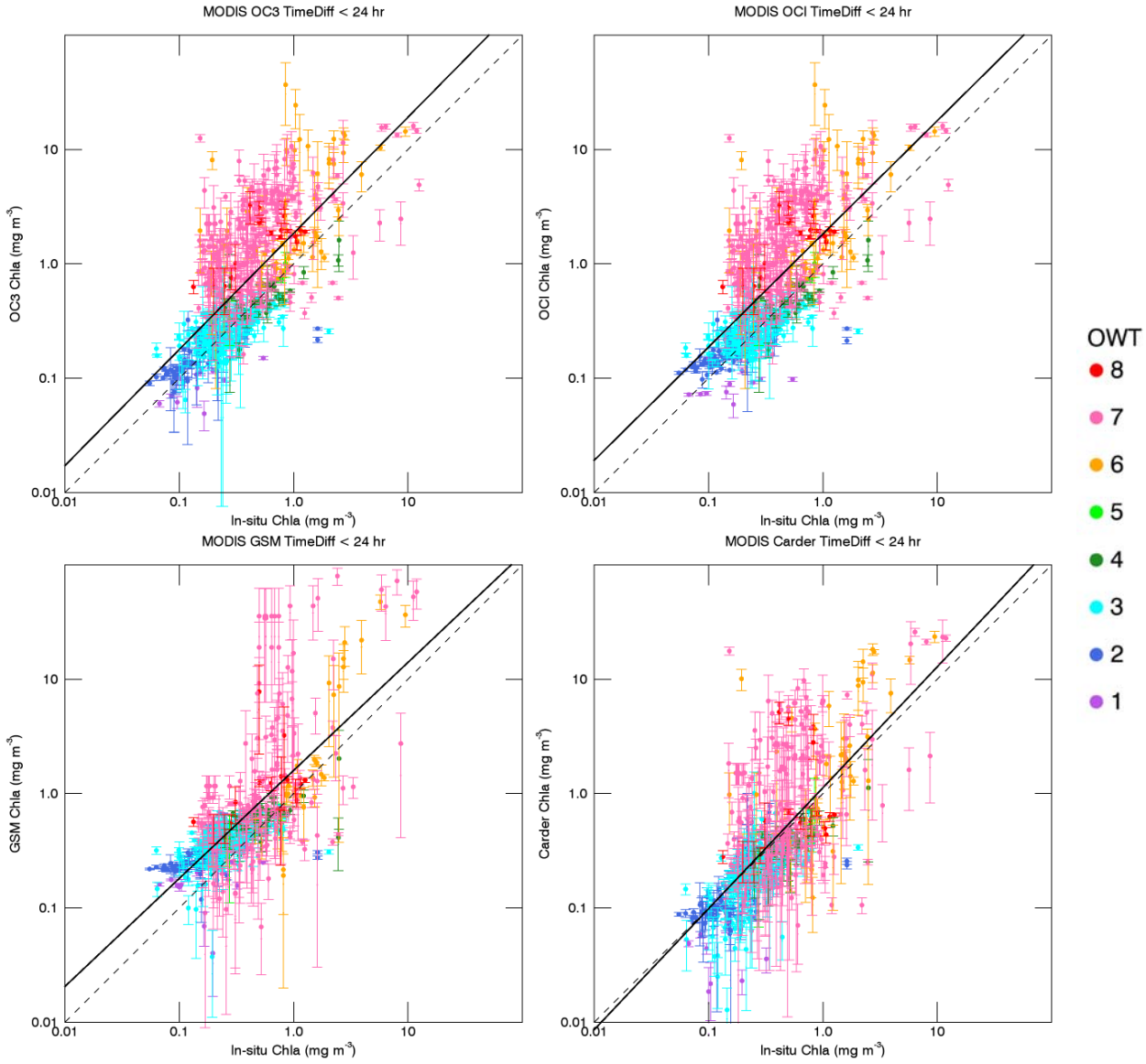

Figure 10 Scatter plots of MODIS-Aqua chl-a match-ups at a maximum time difference of ΔT=±24 h. OWT is indicated by colour. Dashed line is 1:1, solid line is regression for all water types combined. Error bars represent the standard deviation within the match-up area.

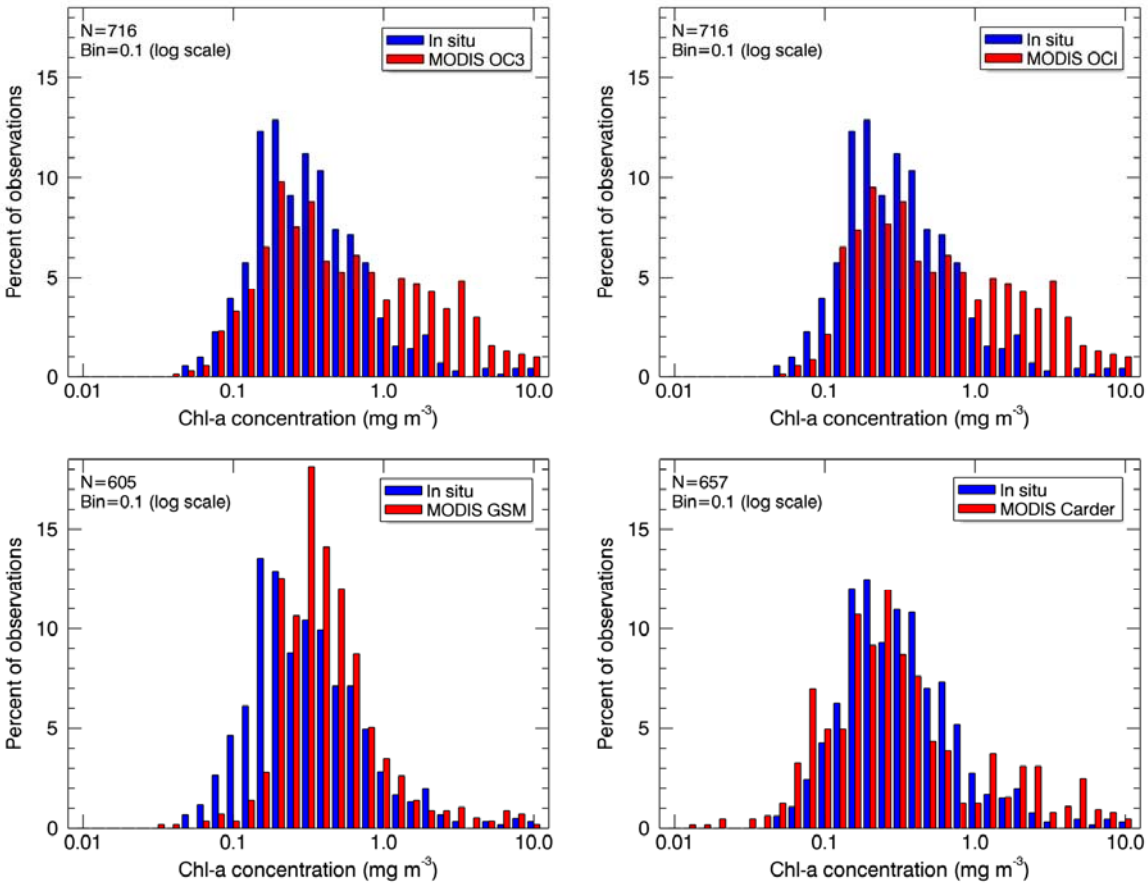

Figure 11 Histograms of chl-a derived from *in situ* and MODIS-Aqua data. Note histogram bins are equal in log-transformed chl-a concentration.

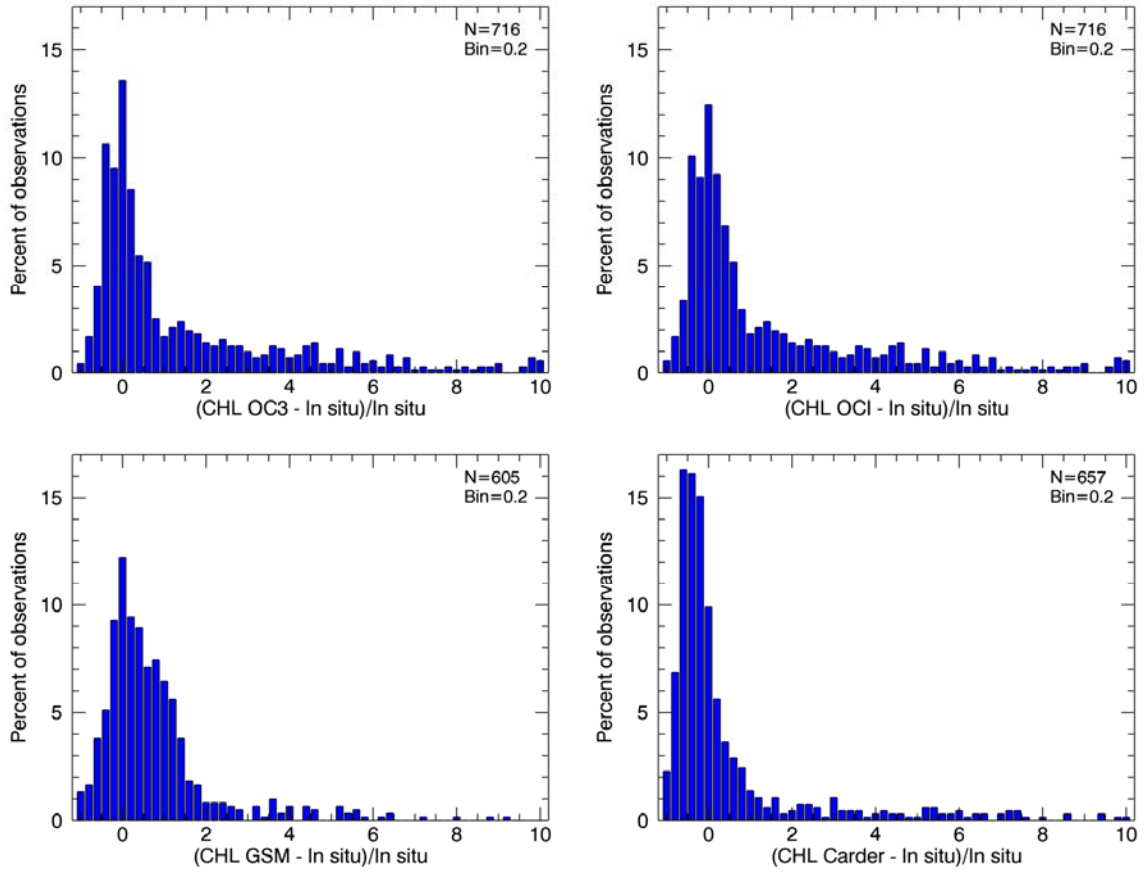

Figure 12 Histograms of the normalised difference chl-a concentration for MODIS-Aqua.

Table 2 Chl-a match-up statistics for the MODIS *OC3* algorithm arranged by Optical Water Type at a maximum time difference of ±24 hours. Correlations marked with ** are statistically significant at the P<0.01 probability while those marked with * are statistically significant at P<0.05.

MODIS-Aqua OC3 ΔT=±24 h								
OWT	**1**	**2**	**3**	**4**	**5**	**6**	**7**	**8**
N	14	74	214	37	3	63	290	19
R^2	0.4804**	0.4709**	0.2536**	0.5358**	0.9428	0.3072**	0.2450**	0.4861**
RMSE	0.3127	0.1882	0.1931	0.1589	0.1186	0.6004	0.6446	0.5411
10^{RMSE}	2.05	1.54	1.56	1.44	1.31	3.98	4.41	3.48
MAPE	36.03	27.90	38.68	26.98	16.17	380.38	380.37	230.01
Bias	-0.2278	0.0162	0.0126	-0.0297	0.0401	0.4265	0.5167	0.4715

Table 3 Same as table 2 but for the MODIS *OCI* algorithm.

MODIS-Aqua OCI ΔT=±24 h								
OWT	**1**	**2**	**3**	**4**	**5**	**6**	**7**	**8**
N	14	74	214	37	3	63	290	19
R^2	0.1028	0.4130**	0.2540**	0.5358**	0.9428	0.3072**	0.2450**	0.4861**
RMSE	0.3636	0.2068	0.1903	0.1589	0.1186	0.6004	0.6446	0.5411
10^{RMSE}	2.31	1.61	1.55	1.44	1.31	3.98	4.41	3.48
MAPE	43.46	36.22	38.44	26.98	16.17	380.38	380.37	230.01
Bias	-0.2264	0.0546	0.0199	-0.0297	0.0401	0.4265	0.5167	0.4715

Table 4 Same as table 2 but for the MODIS *GSM* algorithm.

MODIS-Aqua GSM ΔT=±24 h								
OWT	**1**	**2**	**3**	**4**	**5**	**6**	**7**	**8**
N	14	74	215	37	2	36	211	16
R^2	0.0269	0.2621**	0.2852**	0.3343**	-	0.7479**	0.3204**	0.1697
RMSE	0.3217	0.3312	0.2513	0.1937	-	0.4119	0.6535	0.4697
10^{RMSE}	2.10	2.14	1.78	1.56	-	2.58	4.50	2.95
MAPE	55.85	97.11	65.30	33.49	-	128.74	537.94	190.16
Bias	-0.0260	0.2404	0.1670	0.0494	-	0.1354	0.3447	0.2962

Table 5 Same as table 2 but for the MODIS *Carder* algorithm.

MODIS-Aqua Carder ΔT=±24 h								
OWT	**1**	**2**	**3**	**4**	**5**	**6**	**7**	**8**
N	14	74	213	36	3	51	249	17
R^2	0.1813	0.3552**	0.3387**	0.5656**	0.9340	0.3618**	0.1957**	0.1003
RMSE	0.7908	0.2414	0.2514	0.2004	0.2419	0.5097	0.5471	0.4832
10^{RMSE}	6.18	1.74	1.78	1.59	1.75	3.23	3.52	3.04
MAPE	60.25	32.72	35.24	28.86	24.01	250.29	265.68	182.89
Bias	-0.5372	-0.1007	-0.1153	-0.1429	-0.1025	0.2117	0.1915	0.1533

Table 6 Chl-a match-up statistics for the MODIS *OC3* algorithm arranged by Optical Water Type at a maximum time difference of ±2 hours. Correlations marked with ** are statistically significant at the P<0.01 probability while those marked with * are statistically significant at P<0.05.

MODIS-Aqua OC3 ΔT=±2 h								
OWT	**1**	**2**	**3**	**4**	**5**	**6**	**7**	**8**
N	7	39	125	18	2	40	170	12
R^2	0.8146**	0.5689**	0.2855**	0.1995*	-	0.2678**	0.1529**	0.4236
RMSE	0.4070	0.1749	0.1849	0.1383	-	0.6870	0.6575	0.5910
10^{RMSE}	2.55	1.50	1.53	1.37	-	4.86	4.54	3.90
MAPE	47.85	24.77	37.62	21.10	-	507.62	409.47	254.45
Bias	-0.3090	0.0161	0.0103	-0.0172	-	0.4837	0.5100	0.4966

Table 7 Same as table 6 but for the MODIS *OCI* algorithm.

MODIS-Aqua OCI ΔT=±2 h								
OWT	**1**	**2**	**3**	**4**	**5**	**6**	**7**	**8**
N	7	39	125	18	2	40	170	12
R^2	0.4330	0.4868**	0.2867**	0.1995*	-	0.2678**	0.1529**	0.4236
RMSE	0.5025	0.1945	0.1827	0.1383	-	0.6870	0.6575	0.5910
10^{RMSE}	3.18	1.57	1.52	1.37	-	4.86	4.54	3.90
MAPE	52.55	32.16	37.75	21.10	-	507.62	409.47	254.45
Bias	-0.3622	0.0342	0.0165	-0.0172	-	0.4837	0.5100	0.4966

Table 8 Same as table 6 but for the MODIS *GSM* algorithm.

MODIS-Aqua GSM ΔT=±2 h								
OWT	**1**	**2**	**3**	**4**	**5**	**6**	**7**	**8**
N	7	39	125	18	2	17	122	11
R^2	0.0643	0.3530**	0.3263**	0.3287*	-	0.8660**	0.2070**	0.1113
RMSE	0.3928	0.3137	0.2380	0.1304	-	0.4836	0.6282	0.5515
10^{RMSE}	2.47	2.06	1.73	1.35	-	3.04	4.25	3.56
MAPE	51.52	86.60	60.69	27.39	-	166.55	475.55	242.56
Bias	-0.1011	0.2188	0.1518	0.0719	-	0.1680	0.3238	0.3460

Table 9 Same as table 6 but for the MODIS *Carder* algorithm.

MODIS-Aqua Carder ΔT=±2 h								
OWT	**1**	**2**	**3**	**4**	**5**	**6**	**7**	**8**
N	7	39	124	18	2	28	148	11
R^2	0.4437	0.2853**	0.3897**	0.2664*	-	0.2233*	0.0961**	0.0580
RMSE	0.5419	0.2706	0.2504	0.2205	-	0.5978	0.5650	0.5556
10^{RMSE}	3.48	1.86	1.78	1.66	-	3.96	3.67	3.59
MAPE	51.47	38.27	33.56	30.73	-	359.39	297.96	233.87
Bias	-0.3406	-0.1391	-0.1388	-0.1617	-	0.2569	0.1839	0.2304

Table 10 Chl-a match-up statistics for the MODIS *OC3* algorithm arranged by time difference. Correlations marked with ** are statistically significant at the P<0.01 probability while those marked with * are statistically significant at P<0.05.

MODIS-Aqua OC3					
Time difference	**±24 h**	**±12 h**	**±6 h**	**±3 h**	**±2 h**
N	716	495	464	432	413
R^2	0.4757**	0.4446**	0.4423**	0.4427**	0.4213**
RMSE	0.4755	0.4760	0.4851	0.4891	0.4941
10^{RMSE}	2.99	2.99	3.06	3.08	3.12
MAPE	213.03	221.55	229.85	235.14	240.20
Bias	0.2621	0.2515	0.2615	0.2664	0.2698

Table 11 Same as table 10 but for the MODIS *OCI* algorithm.

MODIS-Aqua OCI					
Time difference	**±24 h**	**±12 h**	**±6 h**	**±3 h**	**±2 h**
N	716	495	464	432	413
R^2	0.4665**	0.4361**	0.4347**	0.4347**	0.4135**
RMSE	0.4765	0.4775	0.4866	0.4906	0.4956
10^{RMSE}	3.00	3.00	3.07	3.09	3.13
MAPE	214.03	222.53	230.66	236.03	241.02
Bias	0.2683	0.2552	0.2647	0.2694	0.2724

Table 12 Same as table 10 but for the MODIS *GSM* algorithm.

MODIS-Aqua GSM					
Time difference	**±24 h**	**±12 h**	**±6 h**	**±3 h**	**±2 h**
N	607	420	389	358	340
R^2	0.4603**	0.4195**	0.4298**	0.4392**	0.4130**
RMSE	0.4498	0.4498	0.4506	0.4482	0.4395
10^{RMSE}	2.82	2.82	2.82	2.81	2.75
MAPE	238.58	244.25	238.98	235.63	221.69
Bias	0.2281	0.2232	0.2209	0.2234	0.2188

Table 13 Same as table 10 but for the MODIS *Carder* algorithm.

MODIS-Aqua Carder					
Time difference	**±24 h**	**±12 h**	**±6 h**	**±3 h**	**±2 h**
N	657	460	427	395	377
R^2	0.4684**	0.4489**	0.4422**	0.4341**	0.4006**
RMSE	0.4219	0.4143	0.4246	0.4287	0.4361
10^{RMSE}	2.64	2.60	2.66	2.68	2.73
MAPE	142.94	150.63	157.94	162.73	168.02
Bias	0.0245	0.0227	0.0254	0.0242	0.0235

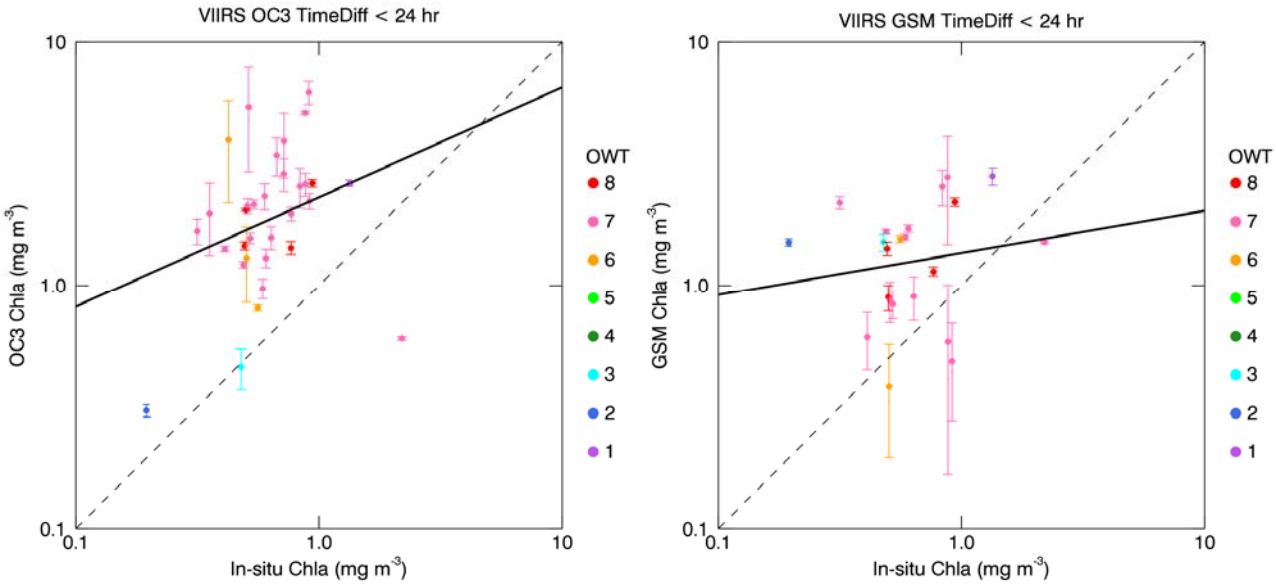

Figure 13 Scatter plots of VIIRS chl-a match-ups, OWT is indicated by colour. Dashed line is 1:1, solid line is regression for all water types combined. Error bars represent the standard deviation within the match-up area.

Table 14 Chl-a match-up statistics for VIIRS match-ups at a maximum time difference of ±24 hours. Correlation coefficients are not statistically significant at the P<0.05 level of probability.

VIIRS	OC3	GSM
N	32	32
R^2	0.0851	0.0232
RMSE	0.5808	0.4439
10^{RMSE}	3.81	2.78
MAPE	269.75	163.20
Bias	0.86	0.3035

A sufficient number of match-ups for VIIRS could only be achieved by allowing a maximum time difference of ±24 h between the *in situ* and satellite observations. The majority of this data is located in optically complex coastal waters represented by OWT6-8. As expected the performance of the empirical *OC3* algorithm was relatively poor as this algorithm was developed for open ocean water application and as such cannot separate the absorption of substances such as CDOM from the absorption of chl-a. In addition the extremely large time differences are inappropriate for match-up comparisons in coastal waters that are often influenced by tidal processes and stronger gradients of optically active constituents resulting in significant ocean colour changes at much shorter time scales (<1h). Consequently *OC3* applied to VIIRS significantly overestimates chl-a compared to the coastal measurements. The performance of the semi-analytical *GSM* is slightly better but due to the large time difference the percentage errors still exceed 160%. A more comprehensive *in situ* data set is required to adequately evaluate the performance of chl-a algorithms for VIIRS.

5 Summary and Recommendations

The accuracy of satellite-derived chl-a products generated and distributed by the IMOS Ocean Colour Sub-facility was evaluated using *in situ* chl-a observations collated by the IMOS Bio-optical Data Base activity. The comparison was performed for the MODIS-Aqua and the Suomi-NPP VIIRS Ocean Colour sensors covering the wider Australasian marine region.

The match-ups between satellite and ground observations were clustered into Optical Water Types that ranged from clear blue open ocean waters to optically complex coastal waters. This water type-based match-up approach provides a useful tool to estimate the accuracy of the satellite Ocean Colour products in regions for which no ground observations exist.

Larger gaps of *in situ* chl-a observations exist for the Great Australian Bight, Bass Strait, Tasman Sea and the Gulf of Carpentaria.

The MODIS *OCI* algorithm does not show an improvement over *OC3* for chl-a concentrations <0.25 mg m^{-3} e.g. less productive waters represented by OWT 1 and 2.

The MODIS *OC3* algorithm was found to be the most accurate chl-a algorithm across Optical Water Types 1-4 showing 21-48% error within ±2 h time difference to the *in situ* observations.

Only a few *in situ* chl-a observations are available for matching MODIS Optical Water Type 5 that represents highly absorbing CDOM-rich waters. More *in situ* measurements of chl-a close to satellite overpasses, for example in Tasmanian coastal waters, are required to fill this gap.

None of the four MODIS chl-a algorithms performed well in coastal waters represented by Optical Water Types 5-8. Percentage errors ranged between 167 and 508% within ±2 h time difference to the ground measurements. All algorithms overestimated chl-a indicated by an average positive bias of up to 0.5 mg m^{-3}.

The number of chl-a match-ups for VIIRS (N=32) were insufficient to allow a clustering into water types. Most *in situ* chl-a measurements for this sensor were collected in optically complex coastal waters. Consequently the performance of the tested *OC3* and *GSM* algorithm were relatively poor also due to the inadequate large time difference of ±24h.

This water-type based validation approach could be extended to other satellite products with a sufficient number of matching ground measurements, such as Total Suspended Solids, as well as inherent and apparent optical properties.

Acknowledgments

We kindly acknowledge the MODIS and VIIRS Characterisation Support Teams and associated NASA and NOAA personnel for their in-orbit sensor calibration efforts.

We also thank the Ocean Biological Processing Group at NASA GSFC, the SeaDAS Development Group at NASA GSFC and Brockmann Consult GmbH for the distribution and maintenance of the SeaDAS software package.

We are grateful to our colleagues Dr David Blondeau-Patissier and Dr Timothy Malthus who helped reviewing this report and acknowledge Paige Kelly for her work on the IMOS Bio-optical Data Base.

All data contributors to the IMOS Bio-optical Data Base are duly acknowledged, explicitly the Australian Institute of Marine Science, James Cook University and the CSIRO.

This research activity was undertaken with the assistance of resources and services from the National Computational Infrastructure (NCI), which is supported by the Australian Government.

Appendix A Symbols and abbreviations

Symbol/abbreviation	Description	Units
a_{CDOM}	Absorption of Coloured Dissolved Organic Matter	m^{-1}
a_d	Absorption of detritus	m^{-1}
a_p	Absorption of particulate matter	m^{-1}
a_{ph}	Absorption of phytoplankton	m^{-1}
chl-a	Chlorophyll-a	mg m^{-3}
TSS	Total Suspended Solids	g m^{-3}
BGCM	Biogeochemical Model	
BODB	Bio-optical Data Base	
CDOM	Coloured Dissolved Organic Matter	
HPLC	High-performance Liquid Chromatography	
IOP	Inherent Optical Property	
MAPE	Mean Absolute Percentage Error	
MODIS	Moderate Resolution Imaging Spectrometer	
NASA	National Aeronautics and Space Administration	
NCI	National Computational Infrastructure	
NOAA	National Oceanic and Atmospheric Administration	
NOMAD	NASA's bio-Optical Marine Algorithm Dataset	
NPP	National Polar-orbiting Partnership	
NRT	Near Real Time	
OCR	Ocean Colour Radiometry	
OWT	Optical Water Type	
PDS	Production Data Set	
SeaDAS	SeaWiFS Data Analysis System	
TERN	Terrestrial Ecosystem Research Network	
RMSE	Root Mean Squared Error	
VIIRS	Visible Infrared Imaging Radiometer Suite	

Appendix B Statistics

The statistical measures used in this report are described by the following equations. In the case of MAPE, *x* is the *in situ* measurement and *y* is the satellite observation and *N* is the number of samples (valid match-ups).

$$MAPE = \frac{100}{N}\sum\frac{|y-x|}{x}$$

For calculation of Bias, RMSE and linear correlation coefficient the input data are log transformed, such that *x* is the $\log_{10}$ of the *in situ* measurement and *y* is the $\log_{10}$ of the satellite observation and *N* is the number of samples (valid match-ups).

$$Bias = \frac{1}{N}\sum(y-x)$$

$$RMSE = \sqrt{\frac{1}{N}(x-y)^2}$$

$$R^2 = \left[\frac{\sum xy - \frac{(\sum x)(\sum y)}{N}}{\sqrt{\left(\sum x^2 - \frac{(\sum x)^2}{N}\right)\left(\sum y^2 - \frac{(\sum y)^2}{N}\right)}}\right]^2$$

Appendix C Data Repositories

The AODN data portal (https://portal.aodn.org.au) is the primary means of discovering and accessing all IMOS satellite data products. The portal allows browsing of the gridded (mapped) products, download of spatio-temporal subsets in netCDF, and access via THREDDS, which supports OPeNDAP.

A copy of all gridded data sets is also held by CSIRO where a THREDDS server supports direct file access, and also the OPeNDAP and OGC Web mapping service protocols (http://rs-data1-mel.csiro.au/imos-srs). An experimental ERDDAP server (created by NOAA in the US) is also available to access selected gridded data products (http://rs-data2-mel.csiro.au/erddap/index.html).

For users requiring direct access to any of the MODIS or VIIRS data sets including the unmapped data in swath format, all data are openly available on the large data storage at the NCI in Canberra, from where they are exposed in the file-system and via WWW and THREDDS servers.

(http://dap.nci.org.au/thredds/remoteCatalogService?catalog=http://dapds00.nci.org.au/thredds/catalog/u39/public/data/catalog.xml)

The IMOS Bio-optical Data Base is available through the AODN portal.

References

Carder K. L., Chen F. R., Lee Z. P., Hawes S. K. and Cannizzaro J. P. (2003), MODIS Ocean Science Team Algorithm Theoretical Basis Document, ATBD 19, Case 2 Chlorophyll a, Version 7, URL: http://modis.gsfc.nasa.gov/data/atbd/atbd_mod19.pdf (accessed 28 August 2014).

Carder K. L., Chen F. R., Lee Z. P., Hawes S. K. and Kamykowski D. (1999), Semianalytic Moderate-Resolution Imaging Spectrometer algorithms for chlorophyll a and absorption with bio-optical domains based on nitrate-depletion temperatures, *Journal of Geophysical Research*: Oceans, 104(C3), 5403-5421.

Fu G., Baith K. S., and McClain C. R. (1998), SeaDAS: The SeaWiFS Data Analysis System, in *Proceedings of the 4th Pacific Ocean Remote Sensing Conference*, Qingdao, China.

Gladkova I., Ignatov A., Shahriar F., Kihai Y., Hillger D., Petrenko B. (2016), Improved VIIRS and MODIS SST imagery, *Remote Sens.,* 8(79), 20.

Hu C., Lee Z., & Franz B. A. (2012), Chlorophyll-a algorithms for oligotrophic oceans: A novel approach based on three-band reflectance difference. *Journal of Geophysical Research*, 117.

IOCCG (2000), Remote Sensing of Ocean Colour in Coastal, and Other Optically-Complex, Waters, Sathyendranath, S. (ed.), Reports of the International Ocean Colour Coordinating Group, No. 3, IOCCG, Dartmouth, Canada.

Jeffrey S. W. & Humphrey G. F. (1975), New spectrophotometric equations for determining chlorophylls *a*, *b*, c_1 and c_2 in higher plants, algae and natural phytoplankton, *Biochemie und Physiologie der Pflanzen,* 167 (2), 191-194.

Maritorena S., Siegel D. A., and Peterson A. R. (2002), Optimization of a semianalytical ocean color model for global-scale applications, *Applied Optics*, 41(15), 2705-2714.

Moore T. S., Campbell J. W. and Dowell M. D. (2009), A class-based approach to characterizing and mapping the uncertainty of the MODIS ocean chlorophyll product, *Remote Sensing of Environment,* 113(11), 2424-2430.

Neveux J., Seppala J. & Dandonneau Y. (2011), Multivariate analysis of extracted pigments using spectrophotometric and spectrofluorometric methods, In *Phytoplankton Pigments:* Characterization, Chemotaxonomy and Applications in Oceanography. Roy, S., Llewellyn, C.A., Egeland, E.S. & Johnsen, G. (eds), Cambridge University Press, New York, 343-371.

O'Reilly J. E., Maritorena S., Siegel D., O'Brien M. O., Toole D., Mitchell B. G., Kahru M., Chavez F. P., Strutton P., Cota G. F., Hooker S. B., McClain C. R., Carder K. L., Muller-Karger F., Harding L., Magnuson A., Phinney D., Moore G. F., Aiken J., Arrigo K. R., Letelier R. M., Culver M. (2000), Ocean Color Chlorophyll a Algorithms for SeaWiFS, OC2, and OC4: Version 4, In SeaWiFS Postlaunch Calibration and Validation Analyses, Volume 11, Part 3, (McClain C. R., Ed.), pages 9-23, Greenbelt, Md.: Goddard Space Flight Center.

Wang, M. and Son S. (2016), VIIRS-derived chlorophyll-a using the ocean color index method, *Remote Sensing of Environment,* 182, 141-149.